

# ON THE CHARACTERISTICS OF INCOMPRESSIBLE TURBULENT BOUNDARY LAYERS

O. Nekhamkina and M. Wolfshtein  
 Technion – Israel Institute of Technology, Haifa, Israel

## Abstract

*Incompressible turbulent boundary layers are discussed. Experimental and Direct Numerical Simulation data for various Reynolds numbers and pressure gradients is compared. The results depict some details of the various parts of the boundary layer, and show some common features of all boundary layers.*

## 1 Introduction

Turbulent boundary layers are important in aerodynamics because a large portion of the drag is generated inside them. Moreover, when subjected to Adverse Pressure Gradient (APG) they may bring about flow separation and stall. The general development of the boundary layer depends on the Reynolds number and the pressure gradient. In general the characteristics of the boundary layer can be predicted using turbulence modeling. However, the quality of the predictions deteriorates when high pressure gradient is considered. Moreover, there is very little data on the changes in the boundary layer when very high Reynolds numbers are considered.

Turbulent models are usually tested against experimental or Direct Numerical Simulation (DNS) data. For best results the data must be detailed and accurate, and it should get sufficiently near to the wall. The available data is limited. Some data refers to low Reynolds number, and some other data does not reach the wall, or does not cover some important quantities (e.g. the viscous dissipation). However, the amount of new data is slowly increasing, and a unified examination of all the available data may expose some trends. This is

important not only in order to understand the phenomena better but also to enable improvements in turbulence modeling.

In this paper we examine some experimental or Direct Numerical Simulation (DNS) data which allows a better understanding of the structure of incompressible turbulent boundary layers in zero and adverse pressure gradients. In particular we seek some common trends and their dependence on the Reynolds number and pressure gradient.

## 2 Definitions

We consider boundary layers in which  $x$  is the stream-wise direction,  $y$  is the direction normal to the wall, and  $z$  is the transverse direction. The corresponding velocity components are respectively  $u$ ,  $v$ , and  $w$ . When needed, an overbar denotes mean values, and a prime denotes a fluctuating quantity.

Traditionally a turbulent boundary layer may be viewed in terms of an inner and outer layers. In the inner layer the velocities are nondimensionalized by  $v^* = \sqrt{\tau_w / \rho}$  and the length is normalized by  $v/v^*$ . In the outer layer the velocities are still normalized by  $v^*$  but the length is normalized by the thickness of the boundary layer. In this work we used the momentum thickness  $\theta$ . The non-dimensional pressure gradient is usually defined in boundary layers in two ways: In the inner layer the definition is

$$P^+ = \frac{v}{\rho v^{*3}} \frac{dp}{dx}$$

related to the inner variables  $v$  and  $v^*$ . In the outer layer the definition is

$$\beta = \frac{\delta^*}{\rho(v^*)^2} \frac{dp}{dx}$$

related to the skin friction and the displacement thickness  $\delta^*$  which is an outer variable.

The length scales of the large (energy carrying) eddies and viscous dissipation,  $L_\mu$  and  $L_\varepsilon$ , may be defined using the relation between the turbulent viscosity  $\nu_t$  and the turbulent kinetic energy dissipation rate  $\varepsilon$  respectively and the turbulent kinetic energy  $k$ . The resulting definitions are

$$L_\mu = \frac{\nu_t}{\sqrt{k}}$$

where

$$\nu_t = \frac{-\overline{u'v'}}{\partial U / \partial y}$$

and

$$L_\varepsilon = \frac{k^{3/2}}{\varepsilon}$$

In some cases the dissipation is not specified in the sources we use. In these cases it is possible to obtain a rough estimate the dissipation by assuming a one-dimensional distribution and a model for the turbulent diffusion of the turbulent energy equation, namely

$$\varepsilon = \frac{\partial}{\partial y} \left[ \left( \nu + \frac{\nu_t}{\sigma_k} \right) \frac{\partial k}{\partial y} \right] + \nu_t \left( \frac{\partial U}{\partial y} \right)^2$$

Two important parameters enable an assessment of the suitability of the data. The distance of the first mesh point from the wall is  $y_1^+$ . Typically this value should be lower than unity in order to allow reliable determination of the structure of the viscous sub layer. The other parameter is  $y_{1d}^+$ , which represents the distance from the wall to the last point which can be assumed to be in the one-dimensional region

near the wall (where the variation in the wall parallel direction can be neglected). This value was estimated by examination of the kinetic energy budget data, seeking the region where the ratio of the convection to dissipation is less than 10 percents.

### 3 Sources

Information about the turbulent properties of incompressible boundary layers has been collated and analyzed by Nekhamkina and Wolfshtein [1], [2]. Data on ZPG (zero pressure gradient) and APG (adverse pressure gradient) turbulent incompressible boundary layer flows was included. This study was based on sets of detailed and reliable experimental or DNS data. The sources of the data are the following:

- Spalart's [3] DNS of ZPG flows denoted as SP88.
- Nagano, Tagawa and Tsuji's [4] experiment of ZPG flows denoted as NTT91.
- Spalart and Watmuff's [5] DNS of APG flows denoted as SW93.
- Nagano, Tagawa and Tsuji's [4] experiment APG flows denoted as NTT91.
- Skaare and Krogstad's [6] experiment APG flow near equilibrium and close to separation denoted as SK94.
- Samuel and Joubert [7] experiment of APG flow denoted as SJ74.

A summary table of all flow is given in Table 1.

It should be noted that:

- (a) The only data in the viscous sub-layer is coming from the DNS data SP88 and SW93;
- (b) The only high Reynolds number flow included is SK94 and SJ74;
- (c) The NT91 data does not include dissipation, which was estimated from the turbulent energy equation.
- (d) The SJ74 data does not approach the wall at all. Therefore the distance of the first point from the wall as well as the

edge of the one-dimensional region are not given.

## 4 Results

Space limitations do not allow a detailed presentation of all results. Therefore only the more interesting results will be shown in figures, while other results will be discussed without the figures.

### 4.1 Velocity Profiles

All cases showed the three typical regions of the velocity profile, namely the linear, logarithmic, and wake region. The best fit for the logarithmic velocity profile was

$$u^+ = 2.439 \ln(y^+) + 5.0718$$

Turbulence models usually predict that  $du^+/dy^+ \propto \sqrt{P^+/y^+}$  in this part of the one-dimensional regions where  $P^+ y^+ \gg 1$ . Examination of the parameters in table 1 shows that these conditions are met only in very few locations. Thus it is not surprising that this region was not clearly identified in the data. However, plotting  $u^+(y^+)$  showed a fairly universal distribution. Near the wall the expected  $du^+/dy^+ = 1$  distribution was found. In larger distance from the wall the expected log region with  $du^+/dy^+ = 1/\kappa y^+$  was evident. However, an intermediate region between the viscous and logarithmic regions with  $du^+/dy^+ = 16/(y^+)^{1.5}$  was evident as well. Near the outer edge of the boundary layer the values drop quickly to zero, as expected. However, in high  $Re_\theta$  and  $\beta$  an additional region is seen, with  $du^+/dy^+ = 0.01$  (Figure 1). In order to confirm the above results we examined also the data of SJ74 for high Reynolds number. The results of the two high Reynolds number flows (SK94 and SJ74) are shown in Figure 2. The distributions of the velocity gradients for

these two sets of data confirm the above discussion. Only the last point in the SJ74 data shows different behavior, but this may be due to end of tunnel effects.

### 4.2 The Turbulent Energy

The turbulent energy showed the expected parabolic profile in the sub-layer for all cases. However, the APG cases showed a ruse in the maximum accompanied by a shift of the position of the maximum to higher  $y^+$ . This was very evident in the plot of  $k^+(y^+)$ . However, the variation in  $\delta^+$  did not allow a convenient display of all the data in one figure. Therefore we decided to show  $k^+(y/\theta)$  in Figure 3. The maximal value of the energy appears to be related to the pressure gradient parameter  $\beta$ . This is evident in Figure 4 showing the relation between the two quantities. Indeed the points appear to follow the formula  $k_{\max} = 7.5 \ln(\beta) - 11.62$ .

In the sub-layer the turbulent energy distribution is parabolic, as predicted by asymptotic theory. A good fit with the data is given by

$$k^+ = 0.16 (y^+)^2$$

It follows that  $\varepsilon_W^+ = 0.32$

### 4.3 The Turbulent Shear Stress

The distribution of the shear stress is shown in Figure 5 below. The distribution near the wall (not shown) behaves like  $y^3$  as expected, and the influence of the pressure gradient on the shear stress is very similar to what was observed in the turbulent energy.

### 4.4 The Bradshaw Constant

The apparent similarity between the turbulent energy and the shear stress immediately poses the question of the behavior of the Bradshaw constant  $a_1 = -\overline{u'v'}/(v^*)^2$ . This quantity is shown in Figure 6 below. It is clear that in the

wall layer  $a_1$  appears to depend on  $y/\theta$ . In the outer part of the boundary layer the scatter of the data points is large, but no consistent dependence on other variables (e.g. the Reynolds number or the pressure gradient) can be identified. A reasonable correlation of  $a_1(y/\theta)$  is

$$a_1 = -\overline{u'v'}/k = \min\{0.28, y/2\theta\}.$$

It may be noted that the value of 0.28 is only 7% below the conventional value of 0.3 recommended by Bradshaw.

#### 4.5 The Dissipation

The distribution of the dissipation in APG boundary layers is shown in Figure 7 below. In a ZPG boundary layer the dissipation in the logarithmic region is known to vary as

$$\varepsilon^+ = \frac{1}{\kappa y^+}$$

The above Figure 7 shows that many of the APG follow this relation as well. Indeed, it is possible that inaccuracies in data processing in the cases that show a different behavior caused this to happen.

#### 4.6 The length scales

For the sake of completeness we repeat here the recommendations of Aupoix et. al. [8]. The length scales (in the "+" system) in the inner layer is given by two formulae. For

$$L_{\mu}^+ = 0.09 \min\left[L_{\mu_0}, 2.5\left(1 + e^{-0.7\beta}\right)\theta^+\right]$$

$$L_{\mu_0} = \begin{cases} 0.0491y^{+2} & y^+ < y_C \\ 2.43y^+ - 30.066 & y_C < y^+ \end{cases}$$

$$y_C = 24.475$$

The dissipative length scale in the inner layer is

$$L_{\varepsilon} = \min\left[L_{\varepsilon_0}, 3\left(1 + e^{-0.5\beta}\right)\theta^+\right]$$

with

$$L_{\varepsilon_0} = \left(C_{\varepsilon_1} + C_{\varepsilon_2}y^+\right) \tanh\left(\frac{C_{\varepsilon_3}y^{+3}}{1 + 0.03y^{+2}}\right)$$

and

$$C_{\varepsilon_1} = 44$$

$$C_{\varepsilon_2} = 2.43\left(1 - e^{-Re_{\theta}/800}\right)$$

$$C_{\varepsilon_3} = 0.2 \frac{1 + 27P^+}{C_{\varepsilon_1}}$$

These definitions allow an estimate of  $k$  and  $\varepsilon$ .

#### 5 Conclusions

Examination of some experimental and DNS data coupled with comparisons of data from various sources suggest that distributions of various turbulent quantities in boundary layer may exhibit somewhat different behavior from the usually expected one. The ratio between the turbulent shear stress and the turbulent energy proposed by Bradshaw appears to be valid for the outer part of APG flows. Near the wall this ratio appears to be linear with  $y/\delta$ . This agrees with asymptotic expansion of the stress and the energy on the wall. The maximal value of the turbulent energy grows very significantly when the pressure gradient parameter  $\beta$  grows. The approximate universality of the  $u^+(y^+)$  in APG flows is worth noting as well. Apart from the logarithmic region which can be identified in all the flows considered other regions were identified as well, namely a power law and a linear region. As additional data becomes available a more extensive study will be required, hopefully with extensions to higher Reynolds numbers.

#### References

- [1] Nekhamkina O and Wolfshtein M, Turbulence length scales distributions in the near-wall region, *Technion - Israel Institute of Technology, Faculty of Aerospace Engineering,*

- TAE Report No. 768, 1996.
- [2] Nekhamkina O and Wolfshtein M, Turbulence length scales distributions in the near-wall region, *Proc. Israel Annual Conf on Aeronautics and Astronautics*, Tel Aviv and Haifa, 1997.
  - [3] Spalart P R, Direct numerical simulations of a turbulent boundary up to  $R_\theta = 1410$ , *Journ of Fluid Mech*, Vol. 187, pp. 61-98, 1988.
  - [4] Nagano Y, Tagawa M and Tsuji T, Effects of adverse pressure gradients on mean flows and turbulence statistics in a boundary layer, *Proceedings of the Eighth Symposium on Turbulent Shear Flows*, Technical University of Munich, pp. 2.3.1 - 2.3.6, September 9-11, 1991.
  - [5] Spalart P R, and Watmuff J H, Experimental and numerical study of a turbulent boundary layer with pressure gradient, *Journ of Fluid Mech*, Vol. 249, pp. 337-371, 1993.
  - [6] Skare P E, and Krogstad P A, A turbulent equilibrium boundary layer near separation, *Journ of Fluid Mech*, Vol. 272, pp. 319-348, , 1994.
  - [7] Samuel A E and Joubert P N, A Boundary Layer Developing in an Increasingly Adverse Pressure Gradient, *Journ of Fluid Mech*, Vol. 66, pp. 481-505, , 1974.
  - [8] Aupoix B, Nekhamkina O and Wolfshtein M, Development And Validation Of A One-Equation Turbulence Model, *Proc 38 Israel Conf on Aerospace Sciences*, pp. 33-44, 1998

#	Author	$Re_\theta$	$C_f * 10^3$	$P^+$	$\beta$	$y_1^+$	$y_{1d}^+$
1.1	SP88	300	5.82	0	0	0.23	80
1.2	SP88	670	4.84	0	0	0.26	150
1.3	SP88	1410	4.13	0	0	0.31	300
2.1	NTT91	1040	4.12	0	0	10.55	400
2.2	NTT91	1330	3.89	0	0	11.17	550
2.3	NTT91	1620	3.71	0	0	8.51	650
2.4	NTT9191	1800	3.78	0	0	11.07	700
3.1	SW93	687.8	4.94	0	0	0.17	90
3.2	SW93	834.7	4.57	0.00804	0.4611	0.16	90
3.3	SW93	914.4	4.35	0.0125	0.7872	0.15	100
3.4	SW93	1076	3.77	0.0177	1.236	0.14	110
3.5	SW93	1545	3.12	0.0204	1.96	0.11	180
4.1	NTT91	1290	3.7	0.009	0.76	9.75	370
4.2	NTT91	1880	2.82	0.018	2.05	9.17	460
4.3	NTT91	2660	2.22	0.023	3.54	8.15	540
4.4	NTT91	3350	1.74	0.025	4.66	8.91	560
5.1	SK94	39120	.590	0.0137	18.5	11.8	1700
5.2	SK94	44420	.585	0.0128	19.3	12.6	2000
5.3	SK94	49180	.567	0.0115	19.0	12.0	2200
5.4	SK94	50980	.546	0.0112	18.9	11.8	2500
6.1	SJ74	4830.935	0.279	0.000352	0.088		
6.2	SJ74	5721.467	0.268	0.000484	0.141		
6.3	SJ74	6434.006	0.25	0.000679	0.215		
6.4	SJ74	7069.892	0.237	0.000916	0.310		
6.5	SJ74	8419.569	0.213	0.001286	0.495		
6.6	SJ74	8976.965	0.204	0.001526	0.617		
6.7	SJ74	9404.063	0.188	0.002	0.825		
6.8	SJ74	10651.5	0.167	0.002926	1.297		
6.9	SJ74	11916.58	0.151	0.004182	2.000		
6.10	SJ74	12448.08	0.135	0.005048	2.416		
6.11	SJ74	13651.64	0.112	0.006392	3.118		
6.12	SJ74	18363.1	00.0685	0.010487	5.738		

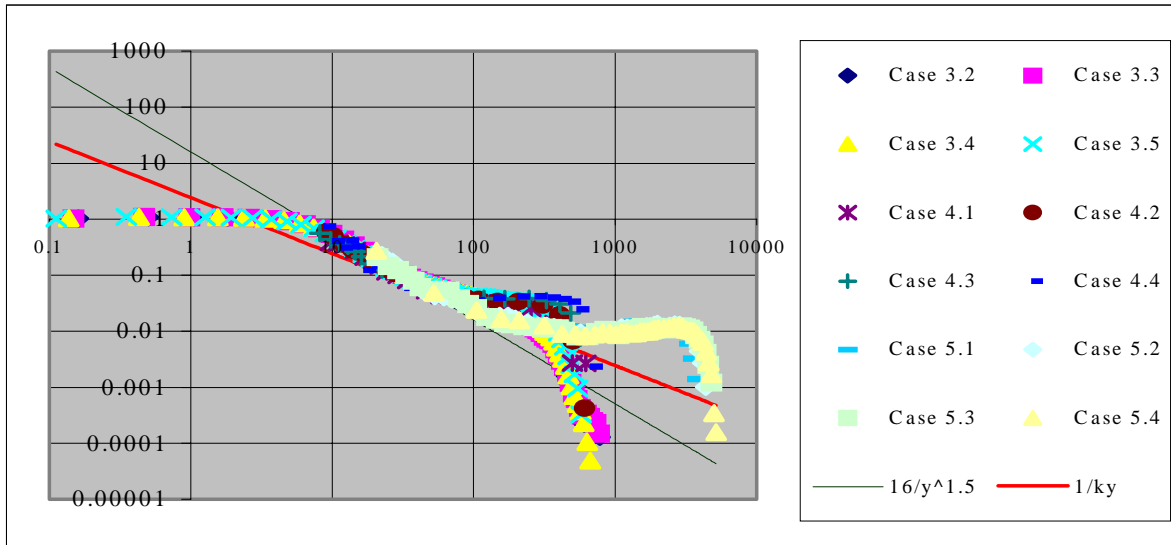


Figure 1:  $u^+$  vs  $y^+$  - APG cases

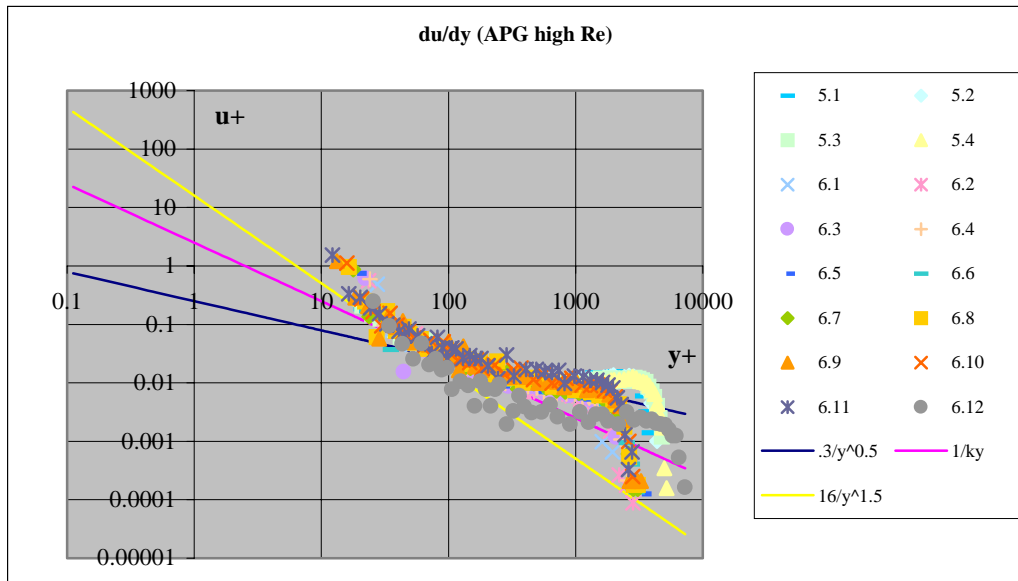


Figure 2 :  $u^+$  vs  $y^+$  - APG high Reynolds number cases

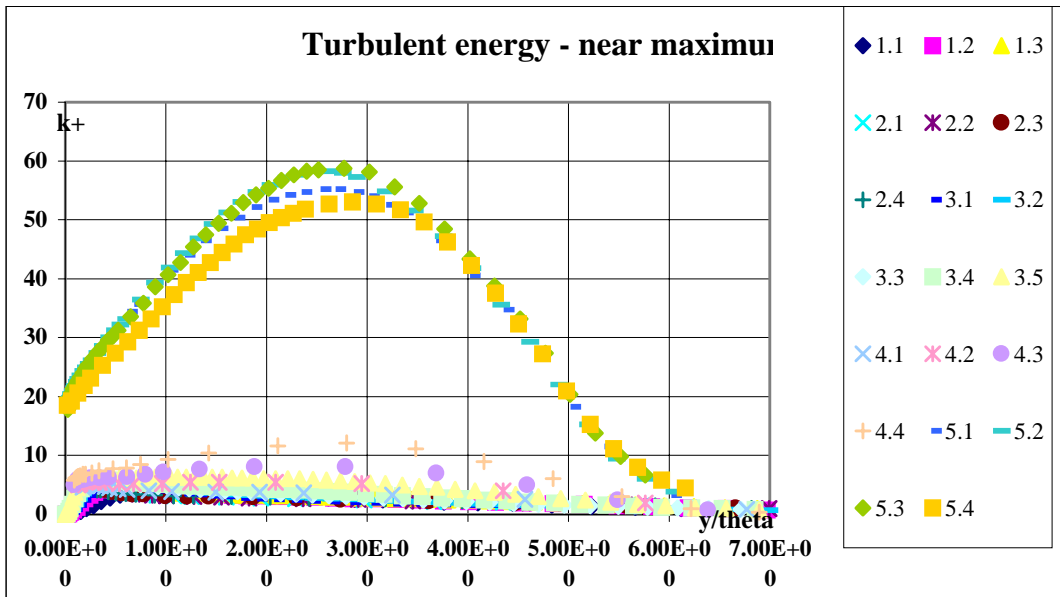


Figure 3: The distribution of  $k^+(y/\theta)$  for ZPG and APG cases across the boundary layer

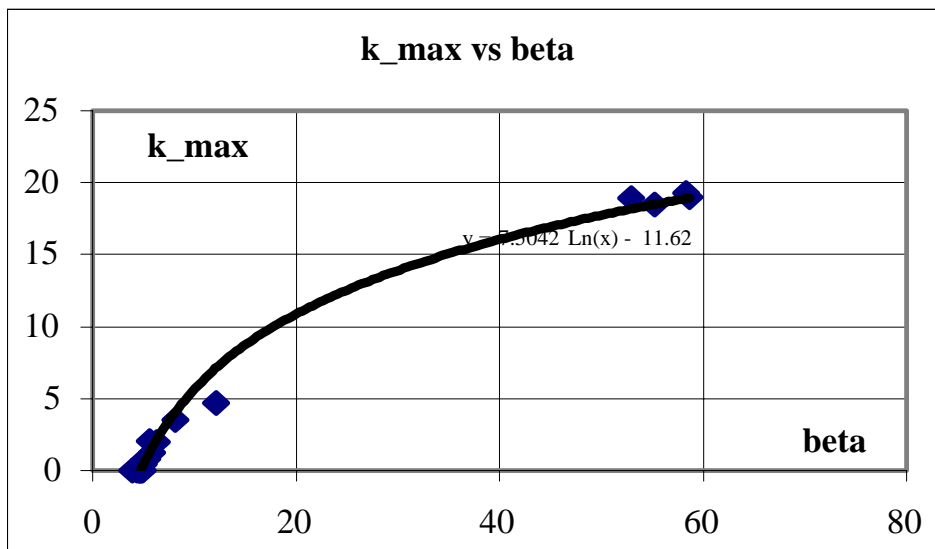


Figure 4: The distribution of  $k^+_{max}(\beta)$

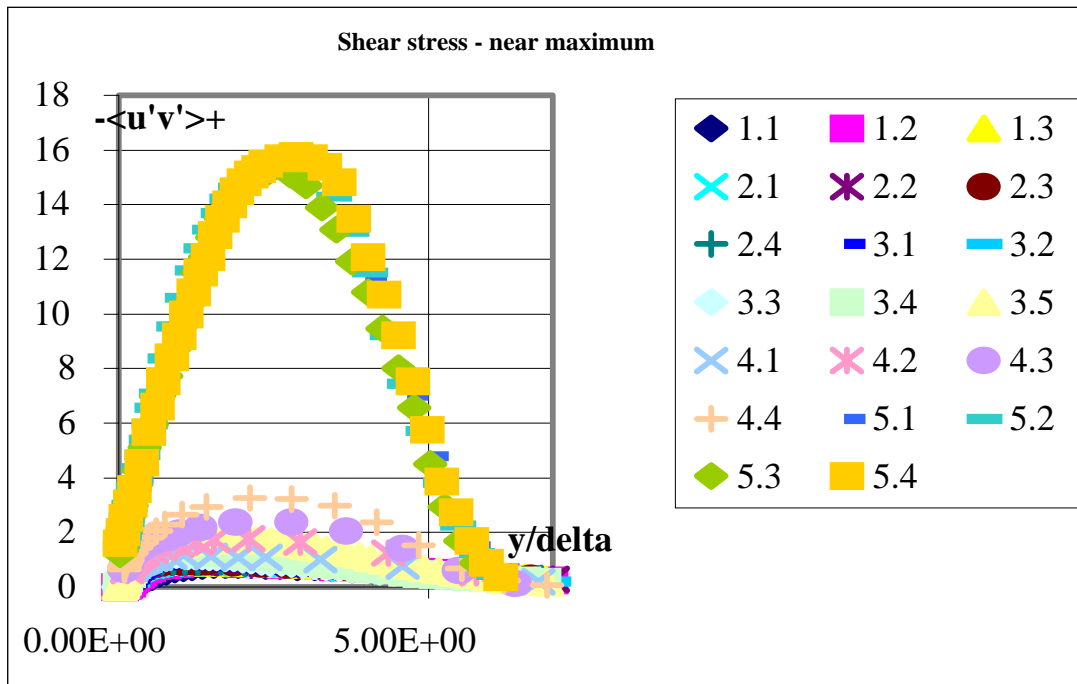


Figure 5: The distribution of  $\tau(y/\theta)$  for ZPG+APG cases across the boundary layer

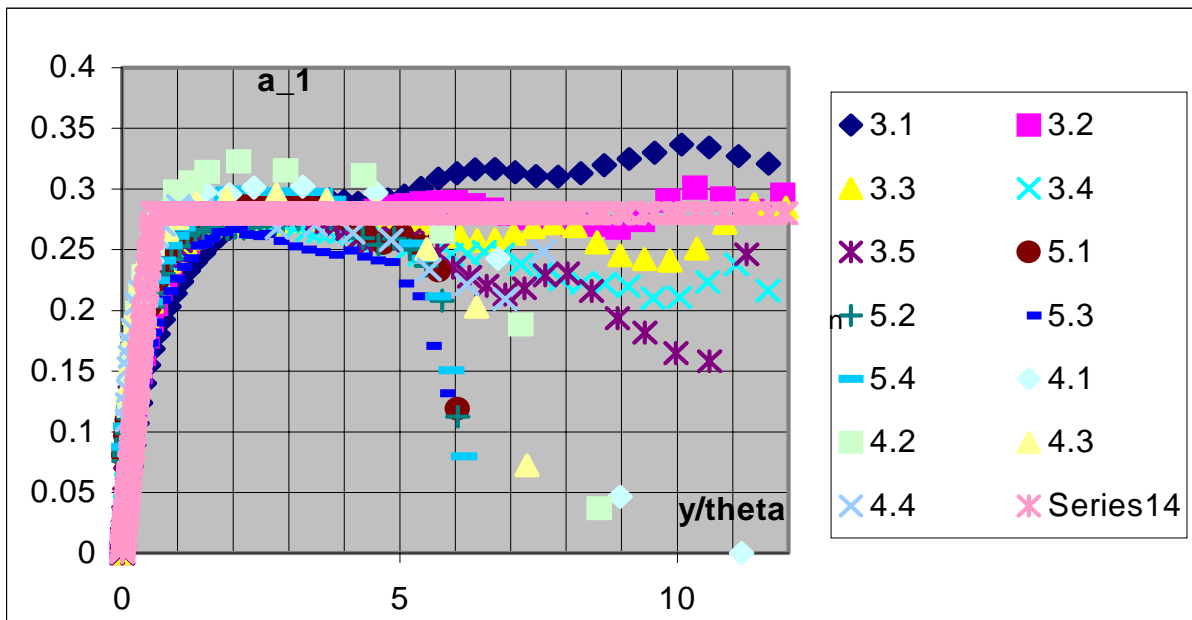


Figure 6: The distribution of  $a_1(y/\theta)$  for APG cases near the wall

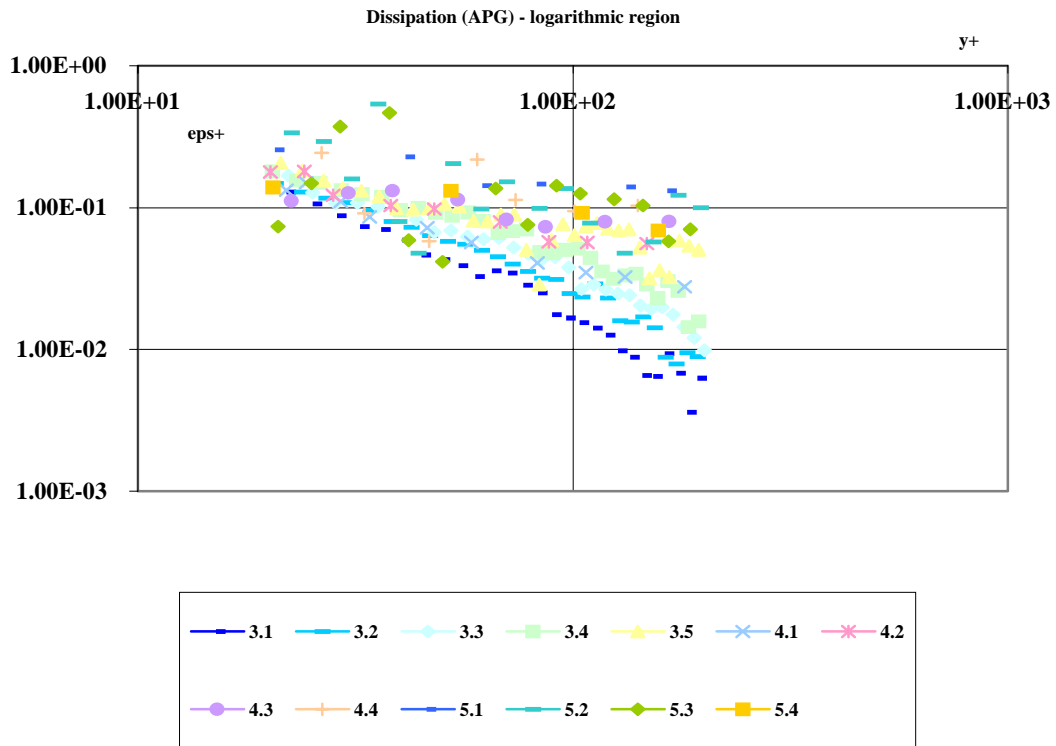


Figure 7: The distribution of  $\varepsilon^+(y^+)$  for APG cases across the boundary layer